

Variable Nanoparticle-Cell Adhesion Strength Regulates Cellular Uptake

Hongyan Yuan,¹ Ju Li,² Gang Bao,³ and Sulin Zhang^{1,*}

¹*Department of Engineering Science and Mechanics, Pennsylvania State University,
University Park, Pennsylvania 16802, USA*

²*Department of Materials Science and Engineering, University of Pennsylvania,
Philadelphia, Pennsylvania 19104, USA*

³*Department of Biomedical Engineering, Georgia Institute of Technology and Emory University,
Atlanta, Georgia 30332, USA*

(Received 20 April 2010; published 21 September 2010)

In receptor-mediated endocytosis, cells exercise biochemical control over the mechanics of adhesion to engulf foreign particles, featuring a variable adhesion strength. Here we present a thermodynamic model with which we elucidate that the variable adhesion strength critically governs the cellular uptake, yielding an uptake phase diagram in the space of ligand density and particle size. We identify from the diagram an endocytosed phase with markedly high uptake, encompassed by a lower and an upper phase boundary that are set, respectively, by the enthalpic and entropic limits of the adhesion strength. The phase diagram may provide useful guidance to the rational design of nanoparticle-based therapeutic and diagnostic agents.

DOI: 10.1103/PhysRevLett.105.138101

PACS numbers: 87.17.Rt, 61.46.Df, 64.70.qd

Inspired by viral invasion of cells [1–3], significant efforts have been recently devoted to the design of synthetic nanoparticles (NPs) as drug carriers and/or imaging contrast agents [4–7]. The NPs are surface coated with ligands (e.g., antibody, peptide, and aptamer) that specifically target surface proteins (receptors) of cancer cells, thereby enhancing therapeutic efficacy and mitigating adverse side effects. Though advanced nanotechnology allows precise control of size, shape, and ligand density of NPs, how these design parameters interrelatedly affect NP-cell adhesion strength and hence the cellular uptake of NPs remains less understood. Experiments *in vitro* showed that the uptake kinetics is strongly dependent on the particle size and shape [8–11]. Analytical models [2,12,13] concerning single NP endocytosis elegantly derived that the endocytic time minimizes at an optimal particle radius of ~ 25 nm, which appears to agree well with experiments. However, the optimal size of the minimal endocytic time may not necessarily correlate to that of the highest uptake rate since the kinetics of simultaneous endocytosis of many NPs might be considerably different from the single-NP models. Statistical thermodynamic models [14,15] shed significant light on the underlying mechanisms of cellular uptake. However, effects of some important design parameters of NPs such as particle size and ligand density appeared not to be the focus of these studies. Hence, it remains unclear what parameter space controls cellular uptake. Identifying the controlling parameter space of NP-cell adhesion is critically important not only for understanding the evolutionary design of viruses, but also for engineering NP-based therapeutic and diagnostic agents and for assessing the toxicity of NPs.

In this Letter, we develop a thermodynamic model with which we elaborate that the adhesion strength between NPs

and the cell is thermodynamically controlled and biochemically regulated. The variable adhesion strength leads to an interrelated effect of particle size and ligand density on the cellular uptake, featuring an uptake phase diagram in the two-parameter space. Through thermodynamic analysis, we identify from the diagram three characteristic phases: an endocytosed phase with high uptake of a couple of thousand, a ligand-shortage phase, and a receptor-shortage phase with vanishing uptake. We reveal that the upper and lower boundaries are, respectively, set by the entropic and enthalpic limits of the adhesion strength. The phase diagram offers a first-hand design map for bioengineering of NPs.

Our thermodynamic model concerns a cell immersed in a solution with dispersed NPs of bulk density φ . We assume that the receptors of an initial surface density ξ_0 are diffusible within the membrane plane. The cross-sectional area of the receptors is A_0 , and hereafter used as the unit area. The NPs are assumed to be spherical and uniformly coated with immobile ligands with a surface density ξ_g . For NPs of radius R , $L = \lfloor K \xi_g \rfloor$ represents the maximal possible number of receptors accessible to each NP, where $K = 4\pi R^2$ is the surface area and the brackets denote taking the floor of the enclosed variable. We assume that at thermodynamic equilibrium N NPs adhere to the membrane with different degrees of wrapping (see Fig. 1). We characterize the degree of wrapping by the fraction of wrapped area, $\eta \equiv k/K \in (0, 1]$, where $k \in (0, K]$ is the wrapped area. We denote by n_{kl} the number of NPs, each of which is wrapped by l receptors with a wrapped area k . A double sum over k and l quantifies the total number of adherent NPs:

$$N = \sum_{k=1}^K \sum_{l=1}^{l_k} n_{kl}, \quad (1)$$

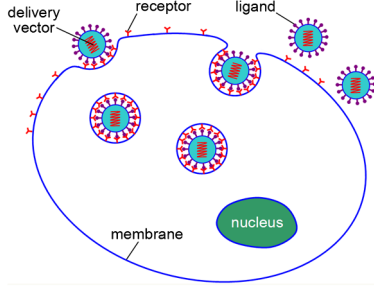


FIG. 1 (color online). Schematic of three possible associations of NPs to the lipid membrane: suspended in solution, partially wrapped with different degrees of wrapping, and endocytosed.

where $l_k = [k\xi_g]$. This two-dimensional (in k and l dimensions) wrapping-size distribution function is different from previous models [2,12,13,15–18] in that the receptor density in NP-membrane bound regions depends on the degree of wrapping. For convenience, we hereafter denote the double summation appeared in Eq. (1) by the symbol \sum_2 . The adherent NPs partition the membrane of a total area M into planar and curved regions. The total bound (curved) membrane area is $M_b = \sum_2 kn_{kl}$, leaving the planar membrane area $M_f = M - M_b$. Conservation of receptors yields

$$M\xi_0 = M_f\xi_f + \sum_2 ln_{kl}, \quad (2)$$

where ξ_f is the receptor density in the planar membrane region. Corresponding to the wrapping-size distribution n_{kl} , a system free energy functional can be written as

$$\begin{aligned} W(n_{kl}) = & M_f[\xi_f \ln \xi_f + (1 - \xi_f) \ln(1 - \xi_f)] \\ & + \sum_2 kn_{kl}\xi_g[(\xi_{kl}) \times \ln(\xi_{kl}) + (1 - \xi_{kl}) \\ & \times \ln(1 - \xi_{kl})] + \sum_2 n_{kl}[\ln(n_{kl}/M) - 1] \\ & - N \ln \varphi - \epsilon \sum_2 ln_{kl} + \sum_2 n_{kl}w_k, \end{aligned} \quad (3)$$

where $\xi_{kl} = l/l_k$. The first two terms in Eq. (3) are the translational entropies of the bound and free receptors, respectively. The third term accounts for the configurational entropy of the 2D mixture of wrapped NPs [15]. The term $-N \ln \varphi$ accounts for the enthalpy change by taking N NPs out of the solution and adhering to the membrane. The term $-\epsilon \sum_2 ln_{kl}$ represents the total binding energy, where ϵ is the binding energy of a ligand-receptor pair. The last term sums up three membrane deformation energies, i.e., $w_k \equiv C_k + \Gamma_k + \Lambda_k$, where C_k and Γ_k are, respectively, the bending and stretching energies stored in the membrane segment adhering to the NP, and Λ_k is the deformation energy stored in the strongly curved membrane detaching from the NP-membrane contact [19]. We note that $C_k = 8\kappa\pi\eta$ is linear in k (or exchangeably η) and $\Gamma_k = k\eta\sigma$ is quadratic in k , where κ is the membrane bending rigidity with units of

energy and σ is the membrane tension. The energy Λ_k is nonlinear in k and vanishes at $\eta = 0$ and $\eta = 1$, resembling an effective capillary energy. Compared to the previous models [14,15,17], the free energy functional treats wrapping-size distribution as a two-dimensional function and introduces ligand density as an additional model parameter, which facilitates the study of interrelated effects of particle size and ligand density.

Minimizing the free energy functional with respect to its independent variables n_{kl} yields

$$n_{kl} = M\varphi e^{k\alpha_{kl} - w_k}, \quad (4)$$

where α_{kl} is naturally defined as the adhesion strength

$$\begin{aligned} \alpha_{kl}(\xi_g; \xi_f) = & \epsilon(l/k) + (l/k) \ln \xi_f + (1 - l/k) \ln(1 - \xi_f) \\ & - \xi_g[\xi_{kl} \ln(\xi_{kl}) + (1 - \xi_{kl}) \ln(1 - \xi_{kl})]. \end{aligned} \quad (5)$$

Taking ξ_g as a prescribed parameter, α_{kl} and hence n_{kl} can be fully determined provided that ξ_f is known. A simple bisection searching scheme is efficient to find ξ_f that satisfies conservations of membrane area and of the receptors. The cellular uptake of our interest is the sum over all the possible $l \in (0, L)$: $n_K = \sum_l n_{kl}$.

Equation (4) shows that NP wrapping size follows a simple Boltzmann distribution with the characteristic energy $\Delta e_{kl} = k\alpha_{kl} - w_k$. This simple expression manifests that NP wrapping is driven by adhesion but penalized by membrane deformation. One notes that the last two terms of the adhesion strength are negligibly small as compared to the first two terms, yielding

$$\alpha_{kl}(\xi_g; \xi_f) \approx \epsilon\xi_{kl}\xi_g + \xi_{kl}\xi_g \ln \xi_f. \quad (6)$$

The first term in Eq. (6) represents the enthalpic component of adhesion strength that locally amounts to the wrapping sites. Whereas the second term represents the entropic penalty that varies with the global distribution of receptors.

From Eq. (4) one identifies the limiting condition under which the cellular uptake vanishes: $\Delta e_{kl} = 0$ for all l . Corresponding to the decomposition of the adhesion strength in Eq. (6), the limiting condition can be approached at critically low enthalpic contribution or large entropic penalty. If neglecting the entropic penalty but considering the local energy balance of a fully wrapped NP, endocytosis would not occur provided that the maximal possible enthalpic adhesion strength $(\alpha_{kl})_{\max} \approx \epsilon\xi_g$ is still insufficient to overcome the membrane deformation cost. The extreme condition yields a lower bound of ligand density

$$\xi_{g,\min} = \frac{1}{\epsilon} \left(\sigma + \frac{2\kappa}{R^2} \right) \quad (7)$$

at fixed R , and a lower bound of particle radius

$$R_{\min} = \sqrt{2\kappa/(\xi_g\epsilon - \sigma)} \quad (8)$$

at fixed ξ_g . Below the lower bounds, cellular uptake vanishes because the NPs are short of ligands (ξ_g is too small). This regime is noted as “ligand-shortage.”

On the other hand, at critically large ligand density or particle size, the receptor density (ξ_f) in the planar membrane region reaches an entropic limit at which adhesion becomes insufficient to overcome membrane deformation cost. The entropic limit gives rise to an upper bound beyond which the cellular uptake vanishes, a regime noted as “receptor shortage.” We resort below to numerical simulations to determining the upper boundary.

In our analysis presented below, we use the thermal energy ($k_B T$) as the unit for all the energy quantities. Our choice of the physical constants is guided by the existing experimental data or literature whenever possible. Unless otherwise explicitly mentioned, we choose $A_0 = 225 \text{ nm}^2$, $\kappa = 20$ [20], $\xi_0 = 0.05$ [21,22], $\epsilon = 20$, $\sigma = 0.225$ [23] ($0.001 k_B T/\text{nm}^2$), $M = 3.14 \times 10^6$ (corresponding to a membrane area of $10 \mu\text{m}$ cell), and $\varphi = 10^{-5}$. All the values without specified units are in reduced units. We systematically computed the cellular uptake as a function of particle radius R and ligand density ξ_g , which allows us to construct a phase diagram on the $R - \xi_g$ plane, as shown in Fig. 2. In the phase diagram, three characteristic regions separated by two phase transition boundaries (dashed and dash-dotted lines) can be identified. Encompassed by the transition boundaries, region II is of markedly high cellular uptake, and therefore noted as the endocytosed phase. In both regions I and III, the cellular uptake vanishes; we denote these two regions, respectively, as “ligand-shortage phase” and “receptor-shortage phase” for the above-mentioned reasons. The lower transition boundary follows well with the enthalpic limit (dotted line) set by Eqs. (7) or (8). In the endocytosed phase, one identifies a subregion

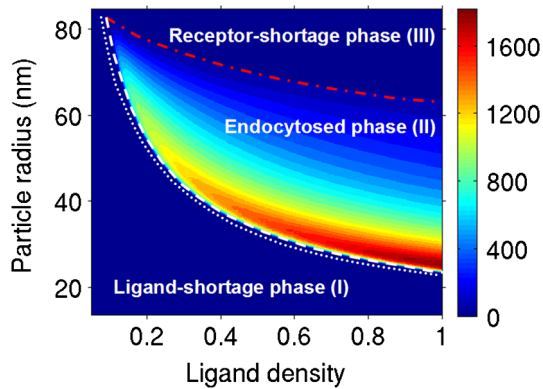


FIG. 2 (color online). A two-dimensional phase diagram on the $(R - \xi_g)$ plane characterizes the interrelated effects of particle size and ligand density on the cellular uptake. The dashed and dash-dotted lines are the lower and upper transition boundaries, respectively. The dotted line represents the theoretical lower bound derived from local wrapping energetics [Eqs. (7) or (8)]. The cellular uptake in the endocytosed phase is markedly high, while those in the other two phases vanish. The color bar indicates the level of cellular uptake.

within which the uptake is noticeably higher. In the sub-region, particle size ranges from 25 to 30 nm in radius, which coincides with both the experimentally determined optimal size [10,11] and that predicted by the kinetic models for minimal endocytic time [8,12,13,24,25]. The cellular uptake in the subregion is on the order of thousands, which also agrees with the experimental data [10,11]. However, since ligand density has been rarely reported in prior experiments, our modeling results thus invite well-controlled experiments for validating the predicted optimal ligand density.

We next elucidate the uptake mechanisms through energetic analysis. Horizontal or vertical cuts of the phase diagram give rise to the representative curves shown in Fig. 3. These curves share similar features: with increasing ξ_g (top panel, at fixed R) or R (bottom panel, at fixed ξ_g), the cellular uptake n_K (solid lines) rises sharply from zero to a peak, and then gradually decreases. For fixed R , the deformation energy cost (w_K) for endocytosing an NP remains constant. As ξ_g exceeds the threshold $\xi_{g,\text{min}}$, endocytosis becomes energetically possible. Increasing ξ_g from $\xi_{g,\text{min}}$ draws more receptors for wrapping, i.e., $d\xi_f \sim -d\xi_g$, thus increasing the entropic penalty. A ligand density only slightly above $\xi_{g,\text{min}}$ causes insignificant change in ξ_f (see supplementary data [26]), and the linear increase of the enthalpic component of the adhesion strength leads to an exponential increase of the cellular uptake towards its maximum according to Eq. (4). Beyond the maximum uptake, further drawing receptors from the free to bound membrane regions becomes entropically very expensive. From Eq. (6), the change in the adhesion strength in this regime can be written as

$$d\alpha_{KI} = (\epsilon + \ln \xi_f) d\xi_g + (\xi_g / \xi_f) d\xi_f. \quad (9)$$

One notes that the first and second terms on the right-hand side of Eq. (9) represent the enthalpic and entropic changes of the adhesion strength, respectively. For small ξ_f , the change of the adhesion strength is entropically dominant.

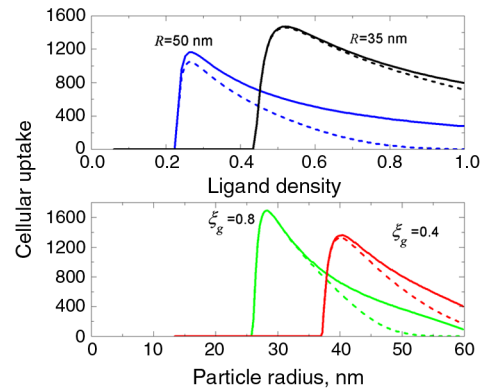


FIG. 3 (color online). The effects of ligand density and particle size on the cellular uptake. All the solid lines represent the total uptake n_K . The dashed lines represent the corresponding uptake contributed by n_{KL} .

As a result, the cellular uptake decreases monotonically with increasing ξ_g .

For fixed ξ_g (bottom panel in Fig. 3), the total number of ligands increases quadratically with increasing R . Following the similar arguments, as R goes slightly beyond the enthalpic threshold R_{\min} , the cellular uptake increases exponentially to its maximum. Further increasing R beyond the maximal uptake would lead to a decrease in ξ_f (see supplementary data [26]), i.e., $d\xi_f \sim -dK$. Since the change in the adhesion strength is entropically dominant, the total adhesion energy $K\alpha_{KL}$ decreases with increasing R : $d(K\alpha_{KL}) = \alpha_{KL}dK + K(\xi_g/\xi_f)d\xi_f < 0$. On the other hand, while the bending energy ($8\pi\kappa$) for endocytosing an NP is independent of R , the stretching energy ($K\sigma$) quadratically scales with R . The decrease of the adhesion energy along with the increase of the deformation energy with increasing R leads to a monotonically decreasing cellular uptake. At a sufficiently large particle size, the cellular uptake vanishes, giving rise to an upper boundary.

Figure 3 also plots the specific term n_{KL} (dashed lines). This term represents the fraction of the uptake for which all the ligands on the NP are bound to receptors. The difference between n_K and n_{KL} indicates the extent to which endocytosis occurs with unbound ligands. A simple analysis reaches the ratio of the consecutive terms $\rho = n_{KL}/n_{K(L-1)} \approx e^{\epsilon + \ln(\xi_f/L)}$. Note that to derive the ratio, the last term in Eq. (5) may no longer be negligible. From our previous analysis, ξ_f monotonically decreases with increasing R and ξ_g . Thus, for small particle size and/or small ligand density $\epsilon \gg |\ln(\xi_f/L)|$ and ρ is very large. In this case, n_{KL} is the leading term of the total uptake, i.e., $n_K \approx n_{KL}$. Oppositely, for large particle size or ligand density, $|\ln(\xi_f/L)|$ is comparable to ϵ and ρ is small. In this case, $n_{KL} \ll n_K$, suggesting endocytosis occurs with considerable unbound ligands [25]. The difference of n_K and n_{KL} plotted in Fig. 3 captures these trends.

We summarize by commenting that the variable adhesion strength originates from the dual character of receptors in endocytosis: providing adhesion energy and at the same time carrying entropic penalty. The variable adhesion strength is tunable through particle size and ligand density, leading to an uptake phase diagram in the two-parameter space. We identify an endocytosed phase with finite uptake, a ligand-shortage phase, and a receptor-shortage phase with vanishing uptake. The sharp transition from the endocytosed phase to the ligand-shortage phase is enthalpy driven, while the gradual transition from the endocytosed phase to the receptor-shortage phase is entropy driven. We further identified an optimal regime of $R \in [25, 30]$ nm and $\xi_g \in [0.8, 1]$ within which the uptake reaches a maximum of a couple of thousand. Both the optimal conditions and the maximal uptake agree with the recent experimental data [10,11]. Our modeling results provide useful guidance for engineering NP-based therapeutic and diagnostic agents.

We thank Dr. Shelly Tzlil, Professor Subra Suresh, and Professor Huajian Gao for helpful discussions. H. Y. and S. L. Z. acknowledge support by NSF. J. L. acknowledges support by NSF, AFSOR, and ONR. G. B. acknowledges support from NIH.

*suz10@psu.edu

- [1] M. Lakadamyali, M. J. Rust, and X. W. Zhuang, *Microb. Infect.* **6**, 929 (2004).
- [2] D. M. Lerner, J. M. Deutsch, and G. F. Oster, *Biophys. J.* **65**, 73 (1993).
- [3] K. Simons and H. Garoff, *J. Gen. Virol.* **50**, 1 (1980).
- [4] S. S. Davis, *Trends Biotechnol.* **15**, 217 (1997).
- [5] F. X. Gu, R. Karnik, A. Z. Wang, F. Alexis, E. Levy-Nissenbaum, S. Hong, R. S. Langer, and O. C. Farokhzad, *Nano Today* **2**, 14 (2007).
- [6] X. Michalet, F. F. Pinaud, L. A. Bentolila, J. M. Tsay, S. Doose, J. J. Li, G. Sundaresan, A. M. Wu, S. S. Gambhir, and S. Weiss, *Science* **307**, 538 (2005).
- [7] M. V. Yezhelyev, X. Gao, Y. Xing, A. Al-Hajj, S. M. Nie, and R. M. O'Regan, *Lancet Oncol.* **7**, 657 (2006).
- [8] M. P. Desai, V. Labhasetwar, E. Walter, R. J. Levy, and G. L. Amidon, *Pharm. Res.* **14**, 1568 (1997).
- [9] Y. Aoyama, T. Kanamori, T. Nakai, T. Sasaki, S. Horiuchi, S. Sando, and T. Niidome, *J. Am. Chem. Soc.* **125**, 3455 (2003).
- [10] B. D. Chithrani, A. A. Ghazani, and W. C. W. Chan, *Nano Lett.* **6**, 662 (2006).
- [11] B. D. Chithrani and W. C. W. Chan, *Nano Lett.* **7**, 1542 (2007).
- [12] H. J. Gao, W. D. Shi, and L. B. Freund, *Proc. Natl. Acad. Sci. U.S.A.* **102**, 9469 (2005).
- [13] G. Bao and X. R. Bao, *Proc. Natl. Acad. Sci. U.S.A.* **102**, 9997 (2005).
- [14] D. van Effenterre and D. Roux, *Europhys. Lett.* **64**, 543 (2003).
- [15] S. Tzlil, M. Deserno, W. M. Gelbert, and A. Ben-Shaul, *Biophys. J.* **86**, 2037 (2004).
- [16] S. X. Sun and D. Wirtz, *Biophys. J.* **90**, L10 (2006).
- [17] S. Zhang, J. Li, G. Lykotrafitis, G. Bao, and S. Suresh, *Adv. Mater.* **21**, 419 (2009).
- [18] W. D. Shi, J. Z. Wang, X. J. Fan, and H. J. Gao, *Phys. Rev. E* **78**, 061914 (2008).
- [19] M. Deserno and T. Bickel, *Europhys. Lett.* **62**, 767 (2003).
- [20] W. Helfrich, *Z. Naturforsch.* **28C**, 693 (1973).
- [21] J. A. G. Briggs, T. Wilk, and S. D. Fuller, *J. Gen. Virol.* **84**, 757 (2003).
- [22] P. Quinn, G. Griffiths, and G. Warren, *J. Cell Biol.* **98**, 2142 (1984).
- [23] M. P. Sheetz, *Nat. Rev. Mol. Cell Biol.* **2**, 392 (2001).
- [24] S. Prabha, W. Z. Zhou, J. Panyam, and V. Labhasetwar, *Int. J. Pharm.* **244**, 105 (2002).
- [25] H. Y. Yuan and S. Zhang, *Appl. Phys. Lett.* **96**, 033704 (2010).
- [26] See supplementary material at <http://link.aps.org/supplemental/10.1103/PhysRevLett.105.138101> for the dependence of the receptor density in the planar membrane region on the particle size and ligand density.